Published in final edited form as:
Invest Ophthalmol Vis Sci. 2009 March ; 50(3): 1205–1214. doi:10.1167/iovs.08-2791.

Lyst Mutation in Mice Recapitulates Iris Defects of Human Exfoliation Syndrome

Colleen M. Trantow[1], **Mao Mao**[1], **Greg E. Petersen**[1], **Erin M. Alward**[1], **Wallace L. M. Alward**[2], **John H. Fingert**[2], and **Michael G. Anderson**[1,2]

1*Department of Molecular Physiology and Biophysics, University of Iowa, Iowa City, Iowa*

2*Department of Ophthalmology and Visual Sciences, University of Iowa, Iowa City, Iowa*

Abstract

Purpose—Human eyes with exfoliation syndrome (XFS) exhibit a distinctive pattern of iris transillumination defects that are recapitulated in *Lyst* mutant mice carrying the *beige* allele. The purpose of this study was to determine the anatomic basis for *Lyst*-mediated transillumination defects, test whether *Lyst* mutant mice develop other features of XFS, and describe the molecular basis of the *beige* mutation.

Methods—*Lyst* mutant mice and strain-matched controls were compared by clinical, histologic, immunohistochemical, and molecular genetic analyses.

Results—Slit-lamp examination showed that *Lyst* mutant mice uniformly exhibit XFS-like transillumination defects. Histologic analysis showed that these defects correlate with a sawtooth morphology of the iris pigment epithelium. *Lyst* mutant mice also produce an exfoliative-like material and exhibit pronounced pigment dispersion. Despite these insults, *Lyst* mutation does not cause increased intraocular pressure or optic nerve damage in the C57BL/6J genetic background. Sequence analysis identified that the *beige* mutation is predicted to delete a single isoleucine from the WD40 domain of the LYST protein, suggesting that this mutation is likely to disrupt a protein-protein interaction.

Conclusions—*Lyst* mutant eyes exhibit multiple features of XFS. Recent human genetic association studies have identified changes occurring in the *LOXL1* gene as an important risk factor for XFS but also indicated that other factors contributing to risk likely exist. These results demonstrated that mutation of the *Lyst* gene can produce ocular features of human XFS and suggested that *LYST* or *LYST*-interacting genes may contribute to XFS.

Exfoliation syndrome (XFS) is a common age-related disorder primarily recognized by the pathologic accumulations of a fibrillar exfoliative material in the anterior chamber of the eye but also associated with several other ocular and systemic abnormalities.[1–6] In many patients, accumulation of exfoliative material within the iridocorneal angle is accompanied by elevated intraocular pressure (IOP) and glaucoma. Indeed, XFS is the most commonly identified cause of secondary open-angle glaucoma.[7]

In parallel to the clinical significance of exfoliative material in the diagnosis of XFS, much of the experimental work on XFS syndrome has focused on studies of exfoliative material. Such studies have shown that exfoliative material consists of an irregular conglomeration of

Corresponding author: Michael G. Anderson, Department of Molecular Physiology and Biophysics, University of Iowa, 6-430 Bowen Science Building, 51 Newton Road, Iowa City, IA 52242; E-mail: michael-g-anderson@uiowa.edu.

Disclosure: **C.M. Trantow**, None; **M. Mao**, None; **G.E. Petersen**, None; **E.M. Alward**, None; **W.L.M. Alward**, None; **J.H. Fingert**, None; **M.G. Anderson**, None

randomly cross-banded fibrils approximately 30 nm in diameter surrounded by an amorphous matrix of glycoconjugates.[8] Exfoliative material also contains epitopes for a variety of proteins related to elastic microfibers, including fibrillin-1,[9] elastin,[10] latent TGF-β proteins,[11] lysyl oxidase,[4] and others.[3,4] These results and other experimental work on XFS have led to a hypothesis that XFS is a disease of elastosis. According to this theory, insults such as increased oxidative stress and elevated levels of TGF-β1 likely trigger increased production of elastic microfibrils that are subsequently prone to aggregate and accumulate.[4] After aggregation and accumulation of exfoliative material within the anterior chamber, aqueous humor outflow becomes impeded, ultimately resulting in increased IOP and glaucoma.

A breakthrough in understanding XFS has been precipitated by genomewide association studies that have begun to unravel the genetic factors underlying XFS. XFS has long been appreciated to have strong hereditary contributions.[12,13] Recently, the lysyl oxidase-like protein 1 gene (*LOXL1*) has been identified as the first known genetic risk factor contributing to XFS.[14] Initially identified from a large genomewide association study among Scandinavian patients with glaucoma[14] and subsequently replicated in additional populations,[15–24] a strong association exists between XFS and two single nucleotide polymorphism (SNP) genetic markers resulting in nonsynonymous changes (rs1048661, R141L; rs3825942, G153D) in *LOXL1*. These *LOXL1* SNPs are highly associated with XFS, and the high-risk alleles of these SNPs occur within most XFS patients. The high-risk haplotype of *LOXL1* alleles has a 99% population attributable risk in Caucasian populations.[14] However, the influence of *LOXL1* in XFS may not be as straightforward as is seemingly indicated by these impressive statistics.

A multifactorial risk for XFS is suggested by the extremely high occurrence of high-risk *LOXL1* alleles among the general population. Within the original Scandinavian populations studied, the high-risk haplotype of *LOXL1* alleles was also detected at a frequency of approximately 50% in the general population, with approximately 25% of the general population homozygous for the haplotype.[14] Follow-up studies have also confirmed similar high-carrier frequencies.[15–24] Thus, most people with high-risk *LOXL1* alleles likely do not have XFS. This indicates that although *LOXL1* is an important risk factor for XFS, additional factors must play a role in the pathogenesis of the condition.

Here, we identify the *Lyst* gene as an additional gene potentially important to XFS. B6-*Lyst*$^{bg\text{-}J}$ mice homozygous for the *beige-J* (*bg-J*) allele recapitulate multiple ocular features of human XFS. Our initial consideration of B6-*Lyst*$^{bg\text{-}J}$ mice as a possible model of XFS was based on a resemblance of iris transillumination defects between these mice and human patients with XFS. In testing the anatomic basis for the *Lyst*-mediated transillumination defects, we found that the transillumination defects were caused by an unusual sawtooth-like morphology of the iris pigment epithelium and were accompanied by the presence of a material resembling human exfoliative material. Interestingly, the molecular basis of the *beige* mutation was discovered to be a 3-bp deletion. The mutation is predicted to delete a single isoleucine from the carboxyl terminus of the LYST protein within the WD40 domain, potentially disrupting a protein-protein interaction. This work represents one of the first descriptions of a mouse model potentially relevant to XFS and provides a genetic resource for continued study of this novel molecular pathway contributing to XFS.

Methods

Mouse Husbandry

C57BL/6J and B6-*Lyst*$^{bg\text{-}J}$/*J* (abbreviated throughout as B6-*Lyst*$^{bg\text{-}J}$) mice were obtained from The Jackson Laboratory (Bar Harbor, ME). All studies of B6-*Lyst*$^{bg\text{-}J}$ mutant mice used homozygotes that were subsequently housed and bred at the University of Iowa Research Animal Facility. Mice were maintained on a 4% fat NIH 31 diet provided ad libitum and were

housed in cages containing dry bedding (Cellu-dri; Shepherd Specialty Papers, Kalamazoo, MI). The environment was kept at 21°C with a 12-hour light/12-hour dark cycle. All animals were treated in accordance with the ARVO Statement for the Use of Animals in Ophthalmic and Vision Research. All experimental protocols were approved by the Animal Care and Use Committee of the University of Iowa.

Human Slit-Lamp Examination

Eyes of patients at the University of Iowa Hospitals and Clinics were photographed using infrared videography, as previously described.[25] Infrared videography has been performed routinely as a clinical diagnostic procedure at the University of Iowa Department of Ophthalmology and Visual Sciences since 1987. This procedure is used on patients with pigment dispersion syndrome, XFS, iris and ciliary body tumors and cysts, and a variety of other anterior segment disorders. University of Iowa Institutional Review Board approval was obtained specifically for evaluating transillumination defects in XFS. All procedures followed the tenets of the Declaration of Helsinki.

Mouse Slit-Lamp Examination

Anterior chamber phenotypes were assayed with a slit-lamp (SL-D7; Topcon, Tokyo, Japan) and photodocumented with a digital camera (D100; Nikon, Tokyo, Japan). For assessment of iris transillumination defects, a small beam of light was shone directly through the undilated pupil of the mouse, and the iris was examined for the ability of reflected light to pass through diseased or depigmented areas of the iris. For assessment of other anterior chamber phenotypes, a beam of light was shone at an angle across the eye, and the anterior chamber was examined for features such as the presence of dispersed pigment, exfoliative material, or cataracts, dimensions of the anterior chamber, iris color and morphology, and other potential findings. Gonioscopy was performed with a 2-mm gonioprism (Ocular Instruments, Bellevue, WA).[26] All ocular examinations were conducted on conscious mice except for gonioscopy, which used mice anesthetized with a mixture of ketamine (100 mg/kg) and xylazine (10 mg/kg). Periodicity of the transillumination defects was measured from digital photographs of B6-*Lyst*$^{bg\text{-}J}$ eyes by measuring the distance between each concentric ring along four radial lines in each eye. All photographs of like kind were taken with identical camera settings and were prepared with identical image software processing.

Immunohistochemistry and Histology

For immunohistochemistry of ocular cryosections, enucleated eyes of age-matched mice were embedded unfixed in optimal cutting temperature embedding medium (Tissue-Tek OCT Compound; Sakura Finetek USA, Torrance, CA), 10-μm sections were cut, and sections were transferred to glass slides (CryoJane, Instrumedics, St. Louis, MO). Cryosections were air dried for 30 minutes at room temperature, fixed for 5 minutes in ice-cold acetone, air dried again for 30 minutes at room temperature, and rehydrated in PBS for 5 minutes. Sections were blocked (15 minutes at room temperature with 1 mg/mL BSA in PBS), labeled with primary antibodies (1 hour at room temperature using polyclonal rabbit anti-fibrillin-1 antibody diluted 1:50; Santa Cruz Biotechnology, Santa Cruz, CA), washed (three washes, 5 minutes each in PBS), and labeled with secondary antibody (1 hour at room temperature using AlexaFluor 488 conjugated antibody diluted 1:200; Invitrogen-Molecular Probes, Carlsbad, CA). After three washes in PBS, the sections were mounted (Vectashield; Vector Laboratories, Burlingame, CA) and were viewed by fluorescence microscopy. All immunohistochemical experiments used assay conditions in which controls using no primary antibody lacked specific signal. For PAS staining, cryosections were fixed as described, subjected to PAS staining, mounted, and viewed on an upright microscope. Periodicity of the sawtooth morphology was measured from images of unfixed cryosections transferred to glass slides as described. Distances were measured

between subsequent troughs of each sawtooth in three to five sections from three B6-*Lyst*$^{bg-J}$ eyes. All photomicrographs were taken with identical camera settings and prepared with identical image software processing.

Transmission Electron Microscopy

Whole eyes of age-matched mice were fixed in 2% formaldehyde, 2.5% glutaraldehyde, 0.25 mg/mL $CaCl_2$, and 100 mM cacodylate buffer (pH 7.4), for at least 24 hours. Eyes were processed for transmission electron microscopy (TEM) using a microwave-assisted double-fixation (aldehyde/osmium), dehydration, and 5-day LR White resin infiltration protocol. After polymerization of the LR White resin, 90-nm sections were cut using an ultramicrotome (EM UC6; Leica, Wetzlar, Germany). After sectioning, staining was performed with uranyl acetate and Reynold lead citrate. Images were recorded with a transmission electron microscope (JEM-1230; JEOL, Tokyo, Japan) equipped with a 2K × 2K CCD camera (USC1000; Gatan, Pleasonton, CA) at the University of Iowa Central Microscopy Core Facility.

IOP Measurement

IOP was measured with a rebound tonometer in accordance with previously described methodology.[27] To summarize, mice were acclimated to the procedure room and anesthetized with 2.5% isoflurane + 100% oxygen. IOP was measured with a tonometer (TonoLab; Colonial Medical Supply, Franconia, NH). Some cohorts included mice measured at more than one age. All IOP cohorts included male and female mice. All measurements were made during the same 2-hour period of the lights-on phase. In sum, this study included IOP measurements from 326 C57BL/6J eyes and 163 B6-*Lyst*$^{bg-J}$ eyes.

Optic Nerve Assessment

Optic nerve cross-sections were examined for glaucomatous damage using a paraphenylenediamine (PPD) staining protocol to stain the myelin sheath of all axons and the axoplasma of damaged axons.[28] Optic nerves were prepared for analysis by overnight fixation in phosphate-buffered glutaraldehyde/paraformaldehyde mixture at 4°C followed by overnight treatment in osmium tetroxide at 4°C. After osmification, nerves were rinsed twice for 10 minutes in 0.1 M phosphate buffer, once in 0.1 M sodium-acetate buffer, and dehydrated in graded ethanol concentrations. After embedding in resin (Eponate-12; Ted Pella, Redding, CA), 1-μm sections were stained in 1% PPD for 35 minutes. Stained sections were compared using a previously described qualitative grading scale to perform quantitative axon counts.[29,30] In short, axons from 18 nonoverlapping fields at 1000× magnification were counted. The images were evenly spread throughout the cross-section of the nerve, and the sum area of these fields was equal to 10% of the total nerve cross-sectional area. *P* values comparing axon counts of B6-*Lyst*$^{bg-J}$ and wild-type optic nerves were determined by two-tailed, heteroscedastic Student's *t*-test.

Sequence Analysis

Because of the large size of the *Lyst* gene (55 known exons spanning 207 kb), we used mRNA rather than genomic DNA to analyze the sequence of the *Lyst* gene. Total RNA was isolated from B6-*Lyst*$^{bg-J}$ mouse spleen (Total RNA Mini Kit; Bio-Rad Laboratories, Hercules, CA), and cDNA was synthesized (iScript cDNA Synthesis Kit; Bio-Rad Laboratories). The entire coding region of the *Lyst* gene was amplified from cDNA as 11 overlapping fragments, including all 55 exons using a long-range PCR reaction (94° for 2 minutes, 40× [94° for 15 seconds, 60° for 1 minute, 68° for 3 minutes], 4°). Primer pairs used in the PCR reactions were as follows: 5′-CCGCTGAGAGAAGTGTTTATGG-3′, 5′-GAACTGCTGGCCACACCTG3′; 5′-ATTGGAAAAAGTTTGTAAGTTTGAC-3′, 5′-TTCTGGCATTGCCTCTGC-3′; 5′-TGATCGCCCCTTTACTGCAT-3′, 5′-CAAATGTGATTTGCAATCTGAATCT-3′; 5′-

CCCTCCCAGTGAGCCATTAAG-3′, 5′-CAGGTCTGGTGCTGTTGCAG-3′; 5′-GGTTTCAGTGGATCGATTGTTTC-3′, 5′-CAAGGAGAAGAATTTCTGTACAAGGAG-3′; 5′-TCAGCATCCTCAAGGGAAAAA-3′, 5′-TTACACGGCATGATGGATGTG-3′; 5′-TGCTGCAGGAACTGTTACTTGAC-3′, 5′-TGCCATCTATGTGCAAAGAGAAGTAG-3′; 5′-TGTGGGAACAGAGCCCAGAT-3′, 5′-TCCTTTTGCTCCTTTGATGCTC-3′; 5′-TTCTCGCAAATTCCCTCTGG-3′, 5′-TTTGAAGCCATCCAACAGATAGG-3′; 5′-GCAGGAATGCATCCAGCAG-3′, 5′-TCGAGCTTTCAACTGCGTCA-3′; 5′-TCACCGGCTTATGTGTCTGC-3′, 5′-GGCACGAGCCTGATCTTTGA-3′. DNA-sequencing reactions were performed by automated fluorescence-tagged sequencing at the University of Iowa DNA Sequencing Facility. Sequencing results were compiled using Sequencher4.1 software and were initially compared to the publicly available C57BL/6J wild-type *Lyst* sequence (NCBI reference sequence, NM010748.2). Confirmatory analysis directly compared DNA sequences from B6-*Lyst*$^{bg\text{-}J}$ and wild-type C57BL/6J mice newly obtained from The Jackson Laboratory. Amino acid numeration used NCBI RefSeq NP_034878.2 as the reference.

Results

Multiple Similarities of *Lyst* Mutant Irides to Human XFS

The *beige* allele of the *Lyst* gene is a spontaneous mutation in mice that was initially identified because of its influence on coat color. Like many mutations influencing coat color, it has subsequently become recognized that the *Lyst* gene influences several additional tissues. Among these, C57BL/6J mice carrying the *beige* allele of the *Lyst* gene (B6-*Lyst*$^{bg\text{-}J}$) exhibit a variety of ocular defects,[31–36] including abnormalities of the iris.[37] To better characterize the pathologic progression of *Lyst*-mediated ocular phenotypes and evaluate potential similarities to human disease, cohorts of B6-*Lyst*$^{bg\text{-}J}$ mice homozygous for the *Lyst*$^{bg\text{-}J}$ mutation were analyzed with an ophthalmic slit lamp (Fig. 1). At all ages examined, B6-*Lyst*$^{bg\text{-}J}$ mice exhibited significant iris defects (n = 30 eyes at 1 to 2 months, 36 eyes at 3 to 6 months, 106 eyes at 7 to 27 months). As we have previously observed,[37] B6-*Lyst*$^{bg\text{-}J}$ mice have a dark gray iris with a dysmorphic iris stroma (Figs. 1A, 1B). Pronounced pigment dispersion was also present. By 3 months of age, pigment dispersion is notable in all eyes, appearing as numerous pigment-laden clump cells across the surface of the iris (Figs. 1C–1F). Interestingly, the extent of pigment dispersion occurring in B6-*Lyst*$^{bg\text{-}J}$ mice is of a magnitude similar to the previously described pigment dispersion phenotype observed in glaucomatous DBA/2J mice.[38] Therefore, we were interested in determining whether B6-*Lyst*$^{bg\text{-}J}$ might also develop other ocular abnormalities relevant to glaucoma.

To test B6-*Lyst*$^{bg\text{-}J}$ mice for potential similarities to secondary forms of glaucoma involving pigment dispersion, we began by assessing mice for iris transillumination defects. In humans, dispersed pigment is a common feature of pigment dispersion syndrome[25,39] and XFS,[40,41] both of which include distinct patterns of iris transillumination defects. Human patients with XFS (Fig. 2) and mice mutant for the *Lyst* gene (Fig. 3) exhibit a unique pattern of concentric periodic iris transillumination defects. This pattern of defects was present in all B6-*Lyst*$^{bg\text{-}J}$ mice examined, was maintained through advanced age, and did not notably worsen in severity (Figs. 3A, 3B). On histologic examination, we found that the origin of this defect likely resides in the iris pigment epithelium, which exhibits an unusual sawtooth-like morphology (Figs. 3C, 3D) with a periodicity matching the iris transillumination defects (Fig. 3E). The pattern of iris transillumination defects in B6-*Lyst*$^{bg\text{-}J}$ mice recapitulates a previously described feature of human XFS.[40,41] The same holds true for the sawtooth-like morphology of the iris pigment epithelium in human eyes from XFS patients.[6,42,43] In sum, the presence of dispersed pigment and the unique pattern of iris transillumination defects in B6-*Lyst*$^{bg\text{-}J}$ mice together led to the hypothesis that B6-*Lyst*$^{bg\text{-}J}$ mice model aspects of XFS.

Accumulations of an Exfoliative Material in *Lyst* Mutant Eyes

Because our slit-lamp examinations suggested that B6-*Lyst*$^{bg-J}$ mice share similarities to XFS, we next set out to determine whether B6-*Lyst*$^{bg-J}$ mice have additional similarities to XFS. The production of exfoliative material in the eye is a classic hallmark of XFS. By slit-lamp examination, we have thus far been unable to detect deposits of exfoliative material in the eyes of B6-*Lyst*$^{bg-J}$ mice. To test for the potential presence of subclinical amounts of exfoliative material, TEM was performed on whole eye samples from wild-type C57BL/6J and mutant B6-*Lyst*$^{bg-J}$ age-matched mice (Fig. 4). Our initial analysis focused on the iris pigment epithelium. Normal eyes from wild-type mice have an iris pigment epithelium with two distinct layers of neuroepithelium-derived pigmented cells bordered anteriorly by a basal lamina facing the iris stroma and posteriorly by a basal lamina facing the lens.[44] The iris pigment epithelium of wild-type C57BL/6J mice was normal, and the basal lamina of the posterior iris pigment epithelium was intact (Fig. 4A). In contrast, the iris pigment epithelium of B6-*Lyst*$^{bg-J}$ mice exhibited several phenotypes. As expected, melanosomes of B6-*Lyst*$^{bg-J}$ mice were enlarged.[32,45] Importantly, the iris pigment epithelium exhibited a sawtooth morphology and was characterized by the presence of accumulations along the surface of the iris pigment epithelium (Fig. 4B). The bush-like aggregates of material in these eyes closely resembled the characteristic accumulations of exfoliative material observed in human XFS.[42] For clarity, we hereafter refer to this material observed in eyes of B6-*Lyst*$^{bg-J}$ mice as exfoliative-like material.

Because we were able to identify exfoliative-like material on the iris pigment epithelium of B6-*Lyst*$^{bg-J}$ mice, we next sought to determine whether this exfoliative-like material was also broadly dispersed in the anterior chamber and in the aqueous humor. To prevent the exfoliative-like material from being disrupted during processing, a slow embedding and infiltration protocol was used on whole eye samples (see Methods). With this technique we identified exfoliative-like material throughout the anterior chamber in B6-*Lyst*$^{bg-J}$ eyes (Fig. 4C). The anterior iris stroma of wild-type C57BL/6J mice appeared normal and intact with two pigmented cell layers (Fig. 4D). In contrast, the anterior iris stroma of mutant B6-*Lyst*$^{bg-J}$ eyes was severely thinned, lacking prominent pigmentation and distinct cell layers. Exfoliative-like material was present within the structures of the iris stroma and along the stromal surface (Figs. 4E, 4F). Because exfoliative-like material was found deep within the iris stroma, one source of this material could be the iris stroma itself, as is seen in human XFS.[42] In sum, these findings indicated that eyes of B6-*Lyst*$^{bg-J}$ mice have multiple similarities to human XFS.

From this TEM analysis, other pathologic features of B6-*Lyst*$^{bg-J}$ eyes were also apparent. First, pigment-engulfed macrophages were present in the anterior chamber and on the surface of the iris stroma of the B6-*Lyst*$^{bg-J}$ eyes (Fig. 4C, arrowhead). Although macrophage involvement has not been described as a prominent feature of human XFS, this phenotype could represent a more subtle aspect of the disease. Second, eyes of B6-*Lyst*$^{bg-J}$ mice contain enlarged melanosomes (Figs. 4B, 4C, 4E). *Lyst* has a well-known role in organelle biogenesis, with known mutations typically resulting in enlarged melanosomes.[32,45] This feature of B6-*Lyst*$^{bg-J}$ eyes does not resemble human XFS and likely represents an independent feature of this allele or of *Lyst* mutant mice in general.

Production of Anti–Fibrillin-1–Positive Material in *Lyst*-Mediated Ocular Disease

As described, results of our TEM analysis demonstrated the presence of exfoliative-like material in B6-*Lyst*$^{bg-J}$ eyes structurally similar to exfoliative material in human XFS. In human eyes, exfoliative material contains epitopes to several components of microfibers, including fibrillin-1.[9] To further characterize potential similarities of the exfoliative-like material in B6-*Lyst*$^{bg-J}$ eyes to human exfoliative material, we performed immunohistochemistry using an anti-fibrillin-1 antibody and frozen cryosections (Fig. 5). We focused our analysis to the anterior chamber structures of mutant B6-*Lyst*$^{bg-J}$ mice and wild-type C57BL/6J control mice

($n = 4$ B6-*Lyst*$^{bg\text{-}J}$ eyes and $n = 3$ C57BL/6J eyes; age 6 months). Viewed by light microscopy, the iris of B6-*Lyst*$^{bg\text{-}J}$ mice appeared dysmorphic compared with C57BL/6J controls, with clumps of pigment and debris evident on the anterior stromal surface (Figs. 5A, 5B). When viewed by fluorescence microscopy, the iris of B6-*Lyst*$^{bg\text{-}J}$ mice had multiple areas of strong labeling corresponding to areas of stromal atrophy and debris accumulation that were positive for fibrillin-1 epitopes, whereas C57BL/6J mice exhibited anti–fibrillin-1 labeling that was primarily limited to the blood vessels of the stroma (Figs. 5C, 5D). In the iridocorneal angle, light microscopy showed that B6-*Lyst*$^{bg\text{-}J}$ eyes had notable accumulations of pigment and debris, whereas the iridocorneal angle of C57BL/6J mice appeared healthy and open (Figs. 5E, 5F). When viewed by fluorescence microscopy, these iridocorneal accumulations of B6-*Lyst*$^{bg\text{-}J}$ eyes included significant amounts of anti–fibrillin-1–positive material (Figs. 5G, 5H). These results demonstrate another similarity between *Lyst*-mediated phenotypes and human XFS; eyes of B6-*Lyst*$^{bg\text{-}J}$ mice accumulate anti–fibrillin-1–positive material in the anterior chamber.

Occluded Iridocorneal Angles in *Lyst* Mutant Eyes

In human XFS, exfoliative material and dispersed pigment tend to accumulate in the iridocorneal angle. In eyes of B6-*Lyst*$^{bg\text{-}J}$ mice, significant accumulations of pigment and debris were also detected within the iridocorneal angle (Fig. 6). By slit-lamp examination, large accumulations were especially pronounced inferiorly (Figs. 6A, 6B). Based on their distinctly rounded appearance at higher magnification, these accumulations appear to largely consist of pigment-laden phagocytic clump cells (Figs. 6C, 6D). To better visualize the relationship of these accumulations to the iridocorneal angle, gonioscopy was performed on a subset of mice ($n = 5$ B6-*Lyst*$^{bg\text{-}J}$ mice, $n = 5$ C57BL/6J controls; age range, 2–12 months). With gonioscopy, the accumulations were readily visible (Figs. 6E, 6F), causing focal occlusion of the iridocorneal angle. On histologic examination, most material in the accumulation appeared to be cellular, with sporadic accumulations of a PAS-positive staining flocculent material that could represent exfoliative-like material (Figs. 6G, 6H). Having visualized these large iridocorneal angle accumulations with multiple techniques, we next set out to address the potential impact on ocular physiology.

Absence of Glaucoma in *Lyst* Mutant Mice on the C57BL/6J Genetic Background

XFS often causes glaucoma in humans. Because the iridocorneal accumulations of B6-*Lyst*$^{bg\text{-}J}$ mice could well impede aqueous humor outflow and elevate IOP, we tested for the presence of glaucoma-related phenotypes in B6-*Lyst*$^{bg\text{-}J}$ mice. To test for increased IOP in B6-*Lyst*$^{bg\text{-}J}$ mice, IOP was evaluated in aging cohorts of B6-*Lyst*$^{bg\text{-}J}$ mice and wild-type C57BL/6J controls ($n = 163$ B6-*Lyst*$^{bg\text{-}J}$ eyes and $n = 326$ C57BL/6J eyes; age range, 1–25 months). The IOP profiles of B6-*Lyst*$^{bg\text{-}J}$ mice indicated that these mice maintained normal IOP compared with wild-type controls (Figs. 7A, 7B). Furthermore, no B6-*Lyst*$^{bg\text{-}J}$ mice had IOP values above 21 mm Hg, a level at which glaucoma is commonly suspected in humans (Figs. 7B, 7C). The nonglaucomatous nature of these values was also confirmed by our analysis of optic nerves (Figs. 7E, 7F). Optic nerve damage was assessed by staining a portion of the retro-orbital optic nerve with PPD (a stain that detects degenerating axons). There was no evidence of glaucomatous optic nerve damage in the mutant B6-*Lyst*$^{bg\text{-}J}$ nerves in comparison with age-matched wild-type C57BL/6J controls ($n = 7$ and 8, respectively; age range, 19–21 months). The density of axons in the mutant B6-*Lyst*$^{bg\text{-}J}$ eyes was 369 ± 43 axons/mm^2 compared with wild-type C57BL/6J control eyes with 374 ± 62 axons/mm^2 ($P = 0.87$). These results indicated that despite the large accumulations of pigment and exfoliative-like material in the iridocorneal angle of B6-*Lyst*$^{bg\text{-}J}$ mice, on the C57BL/6J genetic background *Lyst* mutants do not develop glaucoma.

Identification of *bg-J* Mutation as a 3-bp Deletion in the WD40 Motif

Having identified multiple similarities between human XFS and B6-*Lyst*$^{bg-J}$ mice, we next analyzed the *Lyst* gene to determine the molecular cause of the *bg-J* mutation (Fig. 8). The *bg-J* mutation arose at The Jackson Laboratory as a recessively acting coat color mutation and was first reported in 1962.[46] In subsequent years, *bg-J* was established as an allele of *Lyst* based on complementation assays with molecularly defined alleles. Surprisingly, the molecular cause of the *bg-J* mutation has never been determined. The *Lyst* gene is relatively large, encoding 55 exons and spanning 207 kb. Because of the size of the gene, we began by analyzing known coding regions of the *Lyst* gene by DNA sequencing. This analysis identified a single event in which a 3-bp deletion in exon 54 resulted in the causative mutation. As a consequence of the *Lyst*$^{bg-J}$ mutation, an evolutionarily conserved isoleucine near the carboxyl terminus of the LYST protein was deleted (I3741del). The deletion was predicted to influence the WD40 domain of the LYST protein. Because WD40 domains frequently serve as a stable scaffold for mediating protein-protein interactions,[47] this finding identifies isoleucine 3741 of the LYST protein as a likely candidate for mediating interactions with a key binding partner and provides an important resource for future experiments that might further use this mutation to expand knowledge of LYST-mediated pathways.

Discussion

Mouse models relevant to XFS represent a valuable resource for gaining new insight into mechanisms of this potentially blinding disease.[2] Unfortunately, relatively few, if any, relevant mouse models have previously been described. Here, we have presented multiple lines of evidence that B6-*Lyst*$^{bg-J}$ mice recapitulate several iris defects of human XFS, including a unique pattern of iris transillumination defects associated with a sawtooth morphology of the iris pigment epithelium, the presence of an exfoliative-like material on the iris and elsewhere in the anterior chamber, and pronounced iris pigment dispersion. This constellation of iris phenotypes resembles human XFS. However, it is also important to point out that *Lyst* mutant mice do not resemble human XFS in all regards and that much work remains to complete a framework for understanding these similarities and differences. Nonetheless, the identification that *Lyst* is a genetic factor that can produce features of XFS offers new insight and opportunities for studying this disease.

Mechanisms Underlying XFS

The iris transillumination defects of XFS are distinctive, resembling a series of concentric periodic furrows across the diameter of the iris. Likely because they are best visualized with infrared transillumination, these defects have received relatively little attention in the literature.[40,41] The morphologic basis for this defect has previously not been described. Here, we have shown that the iris pigment epithelium is disrupted, adopting a sawtooth-like morphology that directly correlates with the pattern of iris transillumination defects observed in clinical examinations. Because the periodicity of the histologically identified teeth matches the periodicity of the slit lamp–identified transillumination defects, this likely indicates that the teeth block reflected light whereas the spaces between allow light to pass. At the molecular level, it remains unknown how LYST, or other proteins associated with XFS, might exert this influence over these properties of the iris pigment epithelium. Interestingly, elastic microfibers can serve as substrates for cell adhesion,[48–51] which could have substantial influence on adhesive properties of the posterior iris pigment epithelium. It is, therefore, tempting to speculate that the changes to the iris pigment epithelium described here may be intimately associated with the pathologic changes to microfibers occurring in XFS. Additional experiments will be needed to test this hypothesis directly.

It is unclear how, or whether, LYST pathways might intersect with LOXL1. Recent genetic association studies have identified *LOXL1* sequence variants with increased susceptibility to XFS. However, the same studies also demonstrated that these variant alleles are common among the general population, suggesting that additional risk factors likely remain to be identified. Our current studies identify *LYST* as a worthy candidate for contributing to XFS risk, a hypothesis we are testing. It is also possible that LYST and LOXL1 may interact at the protein level. It is unknown whether the *Lyst* mutation might influence the level, or distribution, of LOXL1 protein or whether the LOXL1 epitope is present in exfoliative-like material in *Lyst* mutant mice. Some binding partners of LYST have been identified,[52] thus far with no evidence that LYST and LOXL1 are likely to directly interact. Interestingly, LYST has been shown to result in altered function of some lysosomal proteins, including elastase.[53] Accordingly, LYST and LOXL1 may interact indirectly through a common pathway influencing elastic microfibers.

Structure and Function of LYST Protein

A second important advance from the current results pertains to structure/function relationships of the LYST protein. Previous studies of the LYST protein have largely focused on its functional role in organelle biogenesis. Independently of our work presented here, *LYST* mutations have been linked with the lethal Chediak-Higashi syndrome.[53] Patients with Chediak-Higashi syndrome typically have various degrees of partial albinism and recurrent pyogenic infections.[54,55] The classic diagnostic feature of Chediak-Higashi syndrome is the presence of giant organelles (including lysosomes, melanosomes, cytolytic granules, and platelet-dense bodies) within various cells of the body. The fact that LYST mutations can influence multiple types of lysosomal-related organelles suggests that the LYST protein likely plays a role at a common point of regulation in their biogenesis. Despite the functional importance of LYST to this important cellular function, relatively little is known concerning precise molecular functions of the wild-type LYST protein.

The LYST protein is a large (430-kDa) protein whose known identifiable motifs are not particularly informative with regard to predicting function. Four protein domains have been identified: an ARM/HEAT domain containing approximately 20 ARM/HEAT repeats (implicated in membrane interactions), a perilipin domain (implicated in interactions with lipid droplets and membranes), a BEACH domain (unknown function, contains the amino acid sequence WIDL), and a WD40 domain containing seven WD40 repeats (protein-protein interaction domain).[56] The LYST protein contains no predicted transmembrane domains and has been shown to be cytosolic with no detectable membrane associations.[57] Likely because the large sizes of the mRNA and protein render them technically difficult to manipulate, relatively few molecular studies of LYST function have been reported.[52,56] In sum, the molecular functions of LYST remain almost completely unknown.

Unfortunately, most genetic studies have contributed relatively little toward an increased molecular understanding of the LYST protein. Nearly all described human *LYST* mutations associated with Chediak-Higashi syndrome lead to protein truncations and likely represent null alleles. As a consequence, genetic studies have generally not contributed to identifying domains of particular functional importance. The exceptions include four different missense mutations in humans that cause an atypical adult-onset form of Chediak-Higashi syndrome.[58,59] Similarly, nearly all described mouse *Lyst* mutations involve truncations or other large deletions and likely also represent null alleles.[35,57,60,61] Exceptions include our description of the *bg-J* allele presented here and the recently described *Ing3618* allele.[61] The *Ing3618* allele involves a missense mutation that, unlike all other known *Lyst* mutations, causes an adult-onset neurodegenerative disease. Like the *bg-J* allele, the $Lyst^{Ing3618}$ mutation is predicted to disrupt the LYST WD40 domain (*Ing3618* disrupts the third WD40 repeat, *bg-J* disrupts the

seventh). Because they disrupt specific residues, both mutations represent valuable new tools for the study of LYST function. In particular, future experiments with these mutations should offer valuable insight toward identification of LYST-interacting proteins that might shed new light on the mechanisms through which LYST contributes to features of XFS and Chediak-Higashi syndrome.

There is little apparent similarity between XFS and Chediak-Higashi syndrome other than that both can involve neurodegenerative stages. For instance, enlarged organelles have not previously been described as a component of human XFS. Conversely, pigment dispersion and exfoliative glaucoma have not been described in patients with Chediak-Higashi syndrome (though early death would likely preclude the ability to observe these late-onset phenotypes). As has been observed in several other patients in whom mutations in one gene can result in more than one disease, we suspect that the phenotypic differences between XFS and Chediak-Higashi syndrome might well be explained by different classes of mutations both influencing *LYST*.

In conclusion, we have presented multiple lines of evidence that B6-*Lyst*$^{bg\text{-}J}$ mice recapitulate the iris defects of human XFS. In building on the results presented here, future experiments with B6-*Lyst*$^{bg\text{-}J}$ mice represent a valuable opportunity to further dissect mechanisms contributing to XFS. In our ongoing work, we intend to extend these initial findings by defining LYST-interacting proteins and testing patients with XFS for disease-causing mutations in *LYST*.

Acknowledgments

The authors thank Adam Hedberg-Buenz for help maintaining the mouse colonies, Katie Striegel for technical contributions to DNA sequencing, and Randy Nessler, along with the University of Iowa Central Microscopy Core, for assistance with the TEM experiments.

Supported by the National Eye Institute Grant EY017673.

References

1. Lahners, W.; Samuelson, TW. Pseudoexfoliative glaucoma. In: Yanoff, M.; Duker, JS., editors. Ophthalmology. St Louis: Mosby; 2004. p. 1499-1503.
2. Ritch R, Schlotzer-Schrehardt U. Exfoliation (pseudoexfoliation) syndrome: toward a new understanding. Proceedings of the First International Think Tank. Acta Ophthalmol Scand 2001;79:213–217. [PubMed: 11284770]
3. Ritch R, Schlotzer-Schrehardt U. Exfoliation syndrome. Surv Ophthalmol 2001;45:265–315. [PubMed: 11166342]
4. Schlotzer-Schrehardt U, Naumann GO. Ocular and systemic pseudoexfoliation syndrome. Am J Ophthalmol 2006;141:921–937. [PubMed: 16678509]
5. Vesti E, Kivel AT. Exfoliation syndrome and exfoliation glaucoma. Prog Retin Eye Res 2000;19:345–368. [PubMed: 10749381]
6. Yanoff, M.; Fine, BS. Ocular Pathology. St. Louis: Mosby; 2002. Lens; p. 339-370.
7. Ritch R. A unification hypothesis of pigment dispersion syndrome. Trans Am Ophthalmol Soc 1996;94:381–405. [PubMed: 8981706]discussion 405–409
8. Davanger M. On the ultrastructure and the formation of pseudoexfoliation material. Acta Ophthalmol (Copenh) 1980;58:520–527. [PubMed: 7193961]
9. Schlotzer-Schrehardt U, von der Mark K, Sakai LY, Naumann GO. Increased extracellular deposition of fibrillin-containing fibrils in pseudoexfoliation syndrome. Invest Ophthalmol Vis Sci 1997;38:970–984. [PubMed: 9112993]

10. Schlotzer-Schrehardt U, Dorfler S, Naumann GO. Immunohistochemical localization of basement membrane components in pseudoexfoliation material of the lens capsule. Curr Eye Res 1992;11:343–355. [PubMed: 1388118]
11. Schlotzer-Schrehardt U, Zenkel M, Kuchle M, Sakai LY, Naumann GO. Role of transforming growth factor-beta 1 and its latent form binding protein in pseudoexfoliation syndrome. Exp Eye Res 2001;73:765–780. [PubMed: 11846508]
12. Gottfredsdottir MS, Sverrisson T, Musch DC, Stefansson E. Chronic open-angle glaucoma and associated ophthalmic findings in monozygotic twins and their spouses in Iceland. J Glaucoma 1999;8:134–139. [PubMed: 10209731]
13. Allingham RR, Loftsdottir M, Gottfredsdottir MS, et al. Pseudoexfoliation syndrome in Icelandic families. Br J Ophthalmol 2001;85:702–707. [PubMed: 11371492]
14. Thorleifsson G, Magnusson KP, Sulem P, et al. Common sequence variants in the LOXL1 gene confer susceptibility to exfoliation glaucoma. Science 2007;317:1397–1400. [PubMed: 17690259]
15. Fingert JH, Alward WL, Kwon YH, et al. LOXL1 mutations are associated with exfoliation syndrome in patients from the midwestern United States. Am J Ophthalmol 2007;144:974–975. [PubMed: 18036875]
16. Hewitt AW, Sharma S, Burdon KP, et al. Ancestral LOXL1 variants are associated with pseudoexfoliation in Caucasian Australians but with markedly lower penetrance than in Nordic people. Hum Mol Genet 2008;17:710–716. [PubMed: 18037624]
17. Hayashi H, Gotoh N, Ueda Y, Nakanishi H, Yoshimura N. Lysyl oxidase-like 1 polymorphisms and exfoliation syndrome in the Japanese population. Am J Ophthalmol 2008;145:582–585. [PubMed: 18201684]
18. Fan BJ, Pasquale L, Grosskreutz CL, et al. DNA sequence variants in the LOXL1 gene are associated with pseudoexfoliation glaucoma in a U.S. clinic-based population with broad ethnic diversity. BMC Med Genet 2008;9:5. [PubMed: 18254956]
19. Yang X, Zabriskie NA, Hau VS, et al. Genetic association of LOXL1 gene variants and exfoliation glaucoma in a Utah cohort. Cell Cycle 2008;7:521–524. [PubMed: 18287813]
20. Challa P, Schmidt S, Liu Y, et al. Analysis of LOXL1 polymorphisms in a United States population with pseudoexfoliation glaucoma. Mol Vis 2008;14:146–149. [PubMed: 18334928]
21. Ramprasad VL, George R, Soumittra N, Sharmila F, Vijaya L, Kumaramanickavel G. Association of non-synonymous single nucleotide polymorphisms in the LOXL1 gene with pseudoexfoliation syndrome in India. Mol Vis 2008;14:318–322. [PubMed: 18334947]
22. Pasutto F, Krumbiegel M, Mardin CY, et al. Association of LOXL1 common sequence variants in German and Italian patients with pseudoexfoliation syndrome and pseudoexfoliation glaucoma. Invest Ophthalmol Vis Sci 2008;49:1459–1463. [PubMed: 18385063]
23. Mossbock G, Renner W, Faschinger C, Schmut O, Wedrich A, Weger M. Lysyl oxidase-like protein 1 (LOXL1) gene polymorphisms and exfoliation glaucoma in a Central European population. Mol Vis 2008;14:857–861. [PubMed: 18483563]
24. Mori K, Imai K, Matsuda A, et al. LOXL1 genetic polymorphisms are associated with exfoliation glaucoma in the Japanese population. Mol Vis 2008;14:1037–1040. [PubMed: 18552979]
25. Alward WL, Munden PM, Verdick RE, Perell HR, Thompson HS. Use of infrared videography to detect and record iris transillumination defects. Arch Ophthalmol 1990;108:748–750. [PubMed: 2334336]
26. Smith RS, Korb D, John SW. A goniolens for clinical monitoring of the mouse iridocorneal angle and optic nerve. Mol Vis 2002;8:26–31. [PubMed: 11889463]
27. Kim CY, Kuehn MH, Anderson MG, Kwon YH. Intraocular pressure measurement in mice: a comparison between Goldmann and rebound tonometry. Eye 2007;21:1202–1209. [PubMed: 16946746]
28. Smith, R.; Zabaleta, A.; John, S., et al. General and special histopathology. In: Smith, RS., editor. Systemic Evaluation of the Mouse Eye. Boca Raton: CRC Press; 2002. p. 265-297.
29. Anderson MG, Libby RT, Gould DB, Smith RS, John SW. High-dose radiation with bone marrow transfer prevents neurodegeneration in an inherited glaucoma. Proc Natl Acad Sci U S A 2005;102:4566–4571. [PubMed: 15758074]

30. Libby RT, Li Y, Savinova OV, et al. Susceptibility to neurodegeneration in a glaucoma is modified by Bax gene dosage. PLoS Genet 2005;1:17–26. [PubMed: 16103918]
31. Collier LL, Bryan GM, Prieur DJ. Ocular manifestations of the Chediak-Higashi syndrome in four species of animals. J Am Vet Med Assoc 1979;175:587–590. [PubMed: 511755]
32. Collier LL, Prieur DJ, King EJ. Ocular melanin pigmentation anomalies in cats, cattle, mink, and mice with Chediak-Higashi syndrome: histologic observations. Curr Eye Res 1984;3:1241–1251. [PubMed: 6488853]
33. Robison WG Jr, Kuwabara T. Light-induced alterations of retinal pigment epithelium in black, albino, and beige mice. Exp Eye Res 1976;22:549–557. [PubMed: 1278263]
34. Robison WG Jr, Kuwabara T, Cogan DG. Lysosomes and melanin granules of the retinal pigment epithelium in a mouse model of the Chediak-Higashi syndrome. Invest Ophthalmol 1975;14:312–317. [PubMed: 1123287]
35. Runkel F, Bussow H, Seburn KL, et al. Grey, a novel mutation in the murine Lyst gene, causes the beige phenotype by skipping of exon 25. Mamm Genome 2006;17:203–210. [PubMed: 16518687]
36. Valenzuela R, Morningstar WA. The ocular pigmentary disturbance of human Chediak-Higashi syndrome: a comparative light- and electron-microscopic study and review of the literature. Am J Clin Pathol 1981;75:591–596. [PubMed: 7223721]
37. Anderson MG, Hawes NL, Trantow CM, Chang B, John SWM. Iris phenotypes and pigment dispersion caused by genes influencing pigmentation. Pigment Cell Melanoma Res 2008;21:565–578. [PubMed: 18715234]
38. Anderson MG, Smith RS, Hawes NL, et al. Mutations in genes encoding melanosomal proteins cause pigmentary glaucoma in DBA/2J mice. Nat Genet 2002;30:81–85. [PubMed: 11743578]
39. Roberts DK, Chaglasian MA, Meetz RE. Iris transillumination defects in the pigment dispersion syndrome as detected with infrared videography: a comparison between a group of blacks and a group of nonblacks. Optom Vis Sci 1999;76:544–549. [PubMed: 10472960]
40. Foos RY. Iris in pseudoexfoliation. Ophthalmology 1991;98:1486–1487. [PubMed: 1961630]
41. Repo LP, Terasvirta ME, Tuovinen EJ. Generalized peripheral iris transluminance in the pseudoexfoliation syndrome. Ophthalmology 1990;97:1027–1029. [PubMed: 2402412]
42. Asano N, Schlotzer-Schrehardt U, Naumann GO. A histopathologic study of iris changes in pseudoexfoliation syndrome. Ophthalmology 1995;102:1279–1290. [PubMed: 9097764]
43. Eagle RC Jr, Font RL, Fine BS. The basement membrane exfoliation syndrome. Arch Ophthalmol 1979;97:510–515. [PubMed: 420639]
44. Smith, RS. The anterior segment and ocular adnexae. In: Smith, RS., editor. Systemic Evaluation of the Mouse Eye. Boca Raton: CRC Press; 2002. p. 366
45. Smith, RS. Choroid, lens, and vitreous. In: Smith, RS., editor. Systemic Evaluation of the Mouse Eye. Boca Raton: CRC Press; 2002. p. 161-193.
46. Lane PW. Bg<2J>—beige-2J. Mouse News Lett 1962;26:35.
47. Smith TF, Gaitatzes C, Saxena K, Neer EJ. The WD repeat: a common architecture for diverse functions. Trends Biochem Sci 1999;24:181–185. [PubMed: 10322433]
48. Bax DV, Mahalingam Y, Cain S, et al. Cell adhesion to fibrillin-1: identification of an Arg-Gly-Asp-dependent synergy region and a heparin-binding site that regulates focal adhesion formation. J Cell Sci 2007;120:1383–1392. [PubMed: 17374638]
49. Chu ML, Tsuda T. Fibulins in development and heritable disease. Birth Defects Res C Embryo Today 2004;72:25–36. [PubMed: 15054902]
50. Kielty CM. Elastic fibres in health and disease. Expert Rev Mol Med 2006;8:1–23. [PubMed: 16893474]
51. Wagenseil JE, Mecham RP. New insights into elastic fiber assembly. Birth Defects Res C Embryo Today 2007;81:229–240. [PubMed: 18228265]
52. Tchernev VT, Mansfield TA, Giot L, et al. The Chediak-Higashi protein interacts with SNARE complex and signal transduction proteins. Mol Med 2002;8:56–64. [PubMed: 11984006]
53. Barbosa MD, Nguyen QA, Tchernev VT, et al. Identification of the homologous beige and Chediak-Higashi syndrome genes. Nature 1996;382:262–265. [PubMed: 8717042]

54. Kaplan J, De Domenico I, Ward DM. Chediak-Higashi syndrome. Curr Opin Hematol 2008;15:22–29. [PubMed: 18043242]

55. Shiflett SL, Kaplan J, Ward DM. Chediak-Higashi syndrome: a rare disorder of lysosomes and lysosome related organelles. Pigment Cell Res 2002;15:251–257. [PubMed: 12100490]

56. Ward DM, Shiflett SL, Huynh D, Vaughn MB, Prestwich G, Kaplan J. Use of expression constructs to dissect the functional domains of the CHS/beige protein: identification of multiple phenotypes. Traffic 2003;4:403–415. [PubMed: 12753649]

57. Perou CM, Leslie JD, Green W, Li L, Ward DM, Kaplan J. The Beige/Chediak-Higashi syndrome gene encodes a widely expressed cytosolic protein. J Biol Chem 1997;272:29790–29794. [PubMed: 9368050]

58. Karim MA, Suzuki K, Fukai K, et al. Apparent genotype-phenotype correlation in childhood, adolescent, and adult Chediak-Higashi syndrome. Am J Med Genet 2002;108:16–22. [PubMed: 11857544]

59. Uyama E, Hirano T, Ito K, et al. Adult Chediak-Higashi syndrome presenting as parkinsonism and dementia. Acta Neurol Scand 1994;89:175–183. [PubMed: 8030398]

60. Perou CM, Justice MJ, Pryor RJ, Kaplan J. Complementation of the beige mutation in cultured cells by episomally replicating murine yeast artificial chromosomes. Proc Natl Acad Sci U S A 1996;93:5905–5909. [PubMed: 8650191]

61. Rudelius M, Osanger A, Kohlmann S, et al. A missense mutation in the WD40 domain of murine Lyst is linked to severe progressive Purkinje cell degeneration. Acta Neuropathol (Berl) 2006;112:267–276. [PubMed: 16791600]

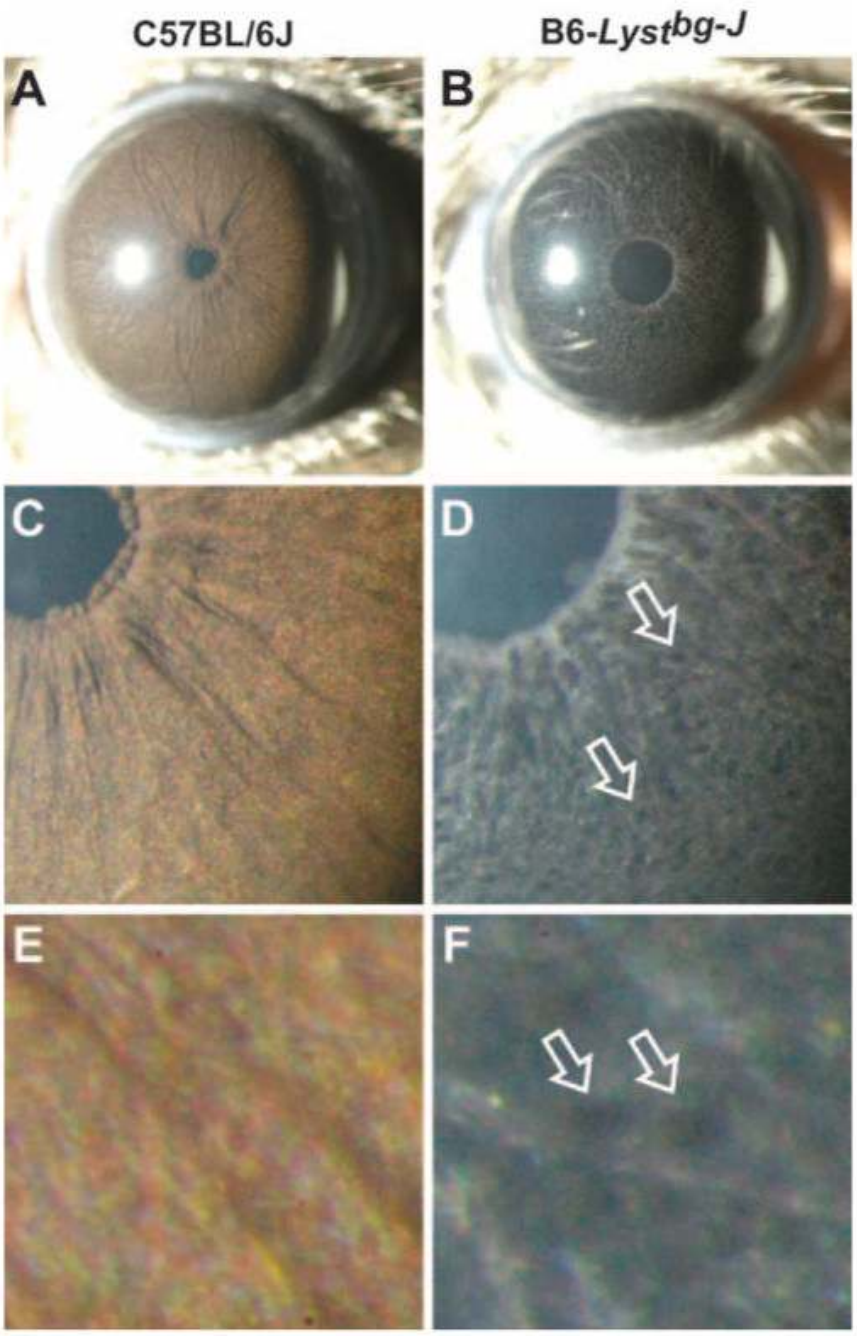

Figure 1.

B6-*Lyst*$^{bg\text{-}J}$ homozygotes have pronounced iris pigment dispersion. Three different slit-lamp images of individual age-matched, 3-month-old wild-type C57BL/6J (*left*) and mutant B6-*Lyst*$^{bg\text{-}J}$ (*right*) eyes. At low magnification, several differences between (**A**) C57BL/6J and (**B**) B6-*Lyst*$^{bg\text{-}J}$ eyes are apparent. The C57BL/6J iris is characterized by a smooth-appearing surface accentuated by numerous underlying vessels and a uniformly deep sienna-brown color. The B6-*Lyst*$^{bg\text{-}J}$ is characterized by pronounced pigment dispersion across the surface of the iris, a roughened appearance to the iris stroma, and a distinctly dark color. At intermediate magnification, finer features of the (**C**) C57BL/6J and (**D**) B6-*Lyst*$^{bg\text{-}J}$ iris become more pronounced. B6-*Lyst*$^{bg\text{-}J}$ eyes have significant pigment dispersion. Small groupings of

pigment-laden clump cells are indicated by *open arrows*; multiple others are visible but unmarked. Indices of a dysmorphic iris stroma include peripupillary atrophy visible as a white ring around the pupil, stromal atrophy visible as streaks of white tissue across the face of the iris, and blood vessels now close enough to the surface of the iris that they appear red. At very high magnification, stromal morphology is accentuated in (**E**) C57BL/6J and (**F**) B6-*Lyst*$^{bg\text{-}J}$ eyes. (**F**) is from the field surrounding the *top open arrow* in (**D**); (**E**) is from an equally sized, analogous midperipheral position of (**C**). Two pigment-laden clump cells (*open arrows*) are clearly visible along a thin vessel in an area of substantial stromal atrophy. (**A**, **B**) Collected with a 25× objective, cropped and reduced. (**C**, **D**) Collected with a 40× objective with less image reduction. (**E**, **F**) Collected with a 40× objective using a 2× magnifying adapter attached to the camera, with slight electronic image enlargement.

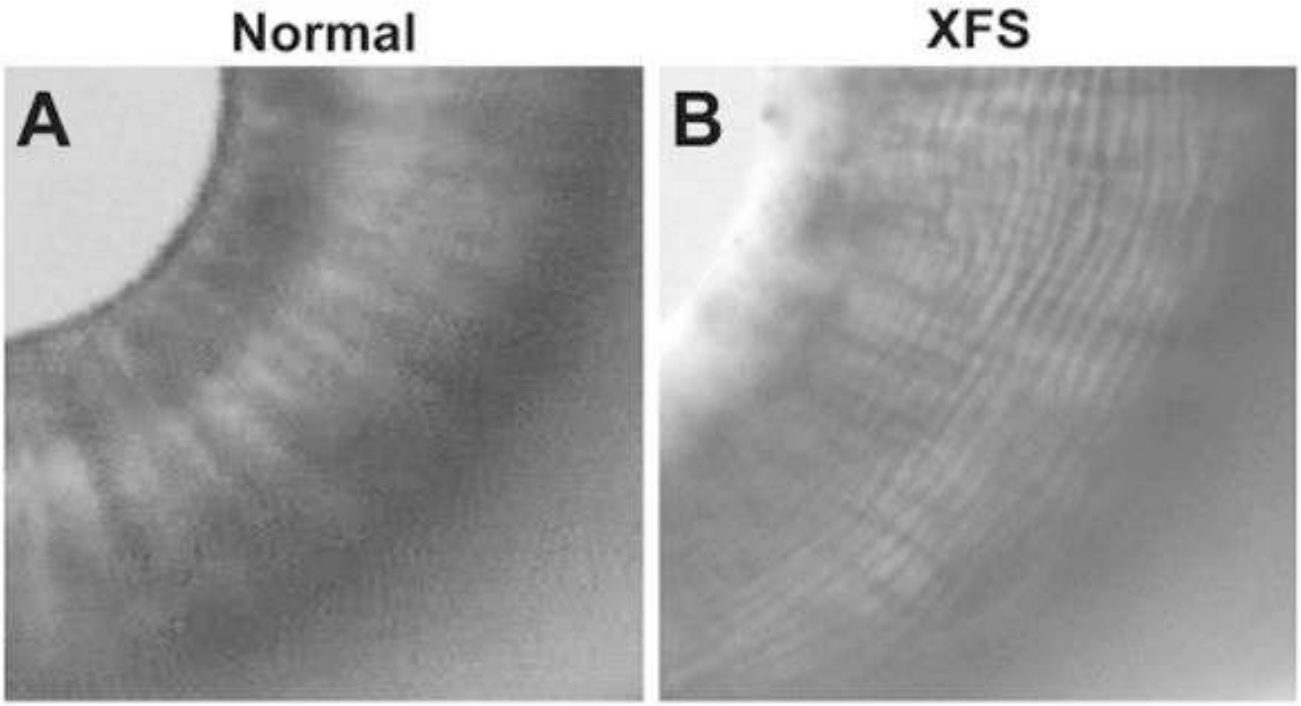

Figure 2.
Human eyes with XFS exhibit a distinct iris transillumination defect. Infrared video images of (**A**) normal and (**B**) XFS eyes showing a unique pattern of concentric periodic iris transillumination defects.

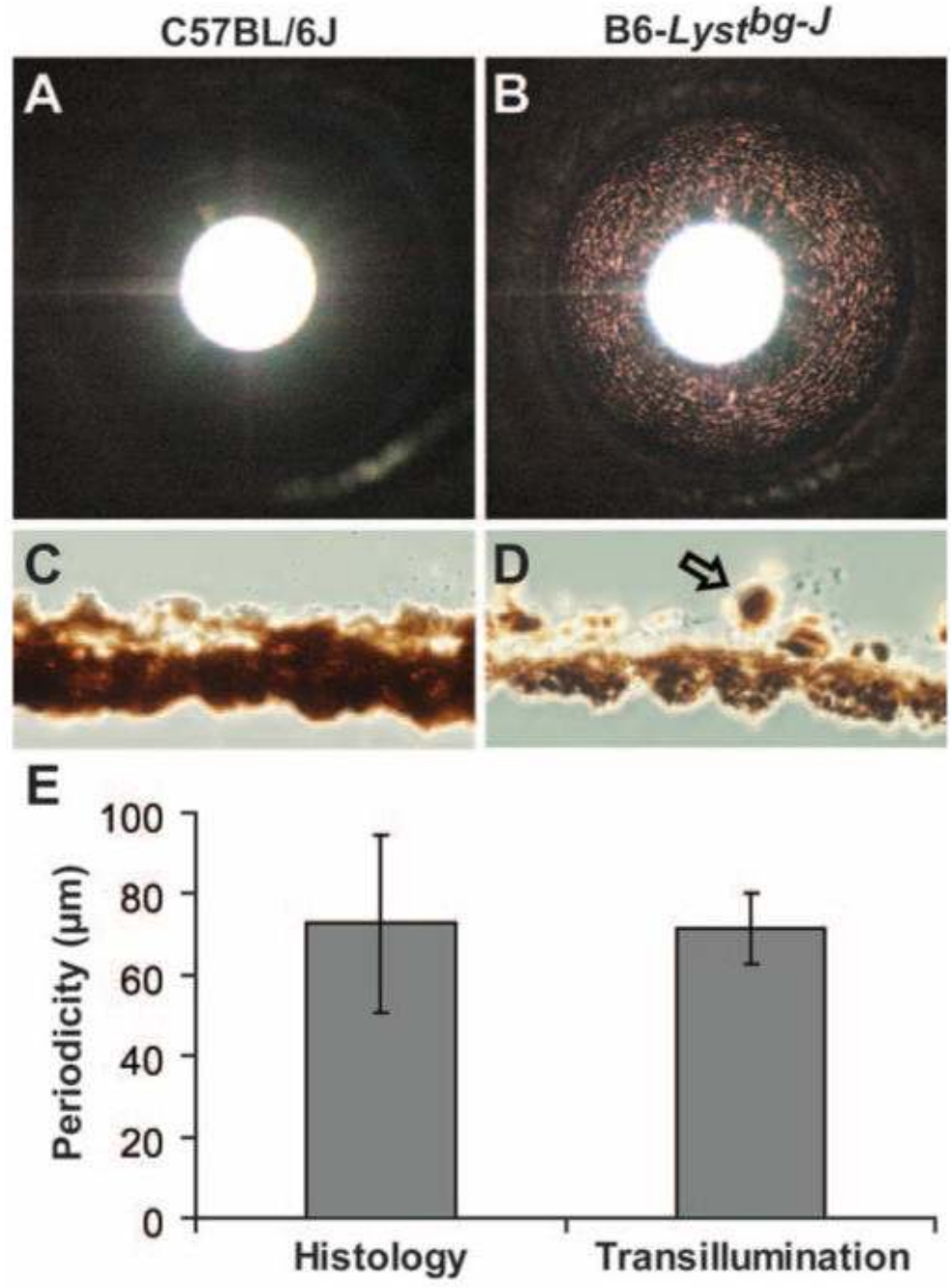

Figure 3.

B6-*Lyst*$^{bg-J}$ homozygotes exhibit a distinct iris transillumination defect. Slit-lamp and histologic images of wild-type C57BL/6J (*left*) and mutant B6-*Lyst*$^{bg-J}$ (*right*) eyes. (**A**) With transilluminating illumination, C57BL/6J irides appear black, indicating an intact healthy iris. (**B**) B6-*Lyst*$^{bg-J}$ eyes show a unique pattern of concentric periodic iris transillumination defects. (**C**) Histologic sections of C57BL/6J irides showing normal iris structure. (**D**) Histologic sections of B6-*Lyst*$^{bg-J}$ irides show a distinct sawtooth morphology of the iris pigment epithelium and a disruption of the iris stroma. One distinctly rounded pigment engulfed macrophage is also visible on the surface of the iris stroma (*arrow*). (**E**) The distance between

the concentric rings of transillumination in B6-*Lyst*$^{bg\text{-}J}$ mice matches the distance between each sawtooth in the iris pigment epithelium of histologic sections (mean ± SD).

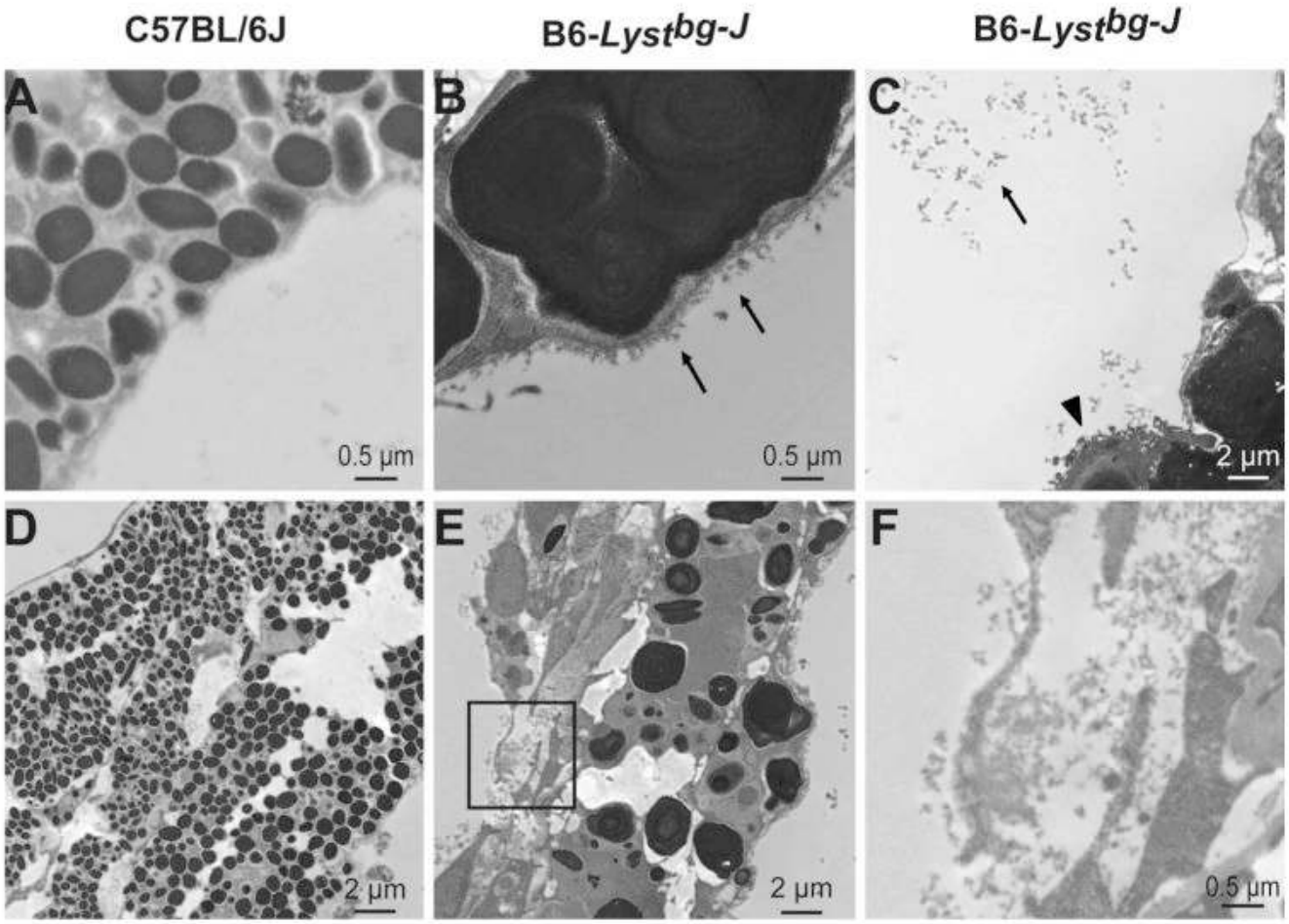

Figure 4.

The anterior chamber of B6-*Lyst*$^{bg\text{-}J}$ homozygotes contains an exfoliative-like material. TEM images of wild-type C57BL/6J (*left*) and mutant B6-*Lyst*$^{bg\text{-}J}$ (*middle*, *right*) structures. (**A**) Normal structure of C57BL/6J posterior iris pigment epithelium. (**B**) B6-*Lyst*$^{bg\text{-}J}$ posterior iris pigment epithelium with exfoliative material accumulating on the surface (*arrows*). (**C**) B6-*Lyst*$^{bg\text{-}J}$ eye with exfoliative material accumulating in the anterior chamber (*arrow*). A portion of a pigment-engulfed macrophage is also visible on the surface of the iris stroma (*arrowhead*). (**D**) Normal structure of the C57BL/6J iris. (**E**) B6-*Lyst*$^{bg\text{-}J}$ iris with exfoliative-like material accumulating in the iris stroma and spilling into the anterior chamber (*box*). (**F**) Enlarged image of the *boxed area* in (**E**). All images were taken of age-matched 12- to 24-month-old mice. Note that enlarged melanosomes are an independent feature of this *Lyst* allele and that (**A**) and (**B**) are at the same magnification.

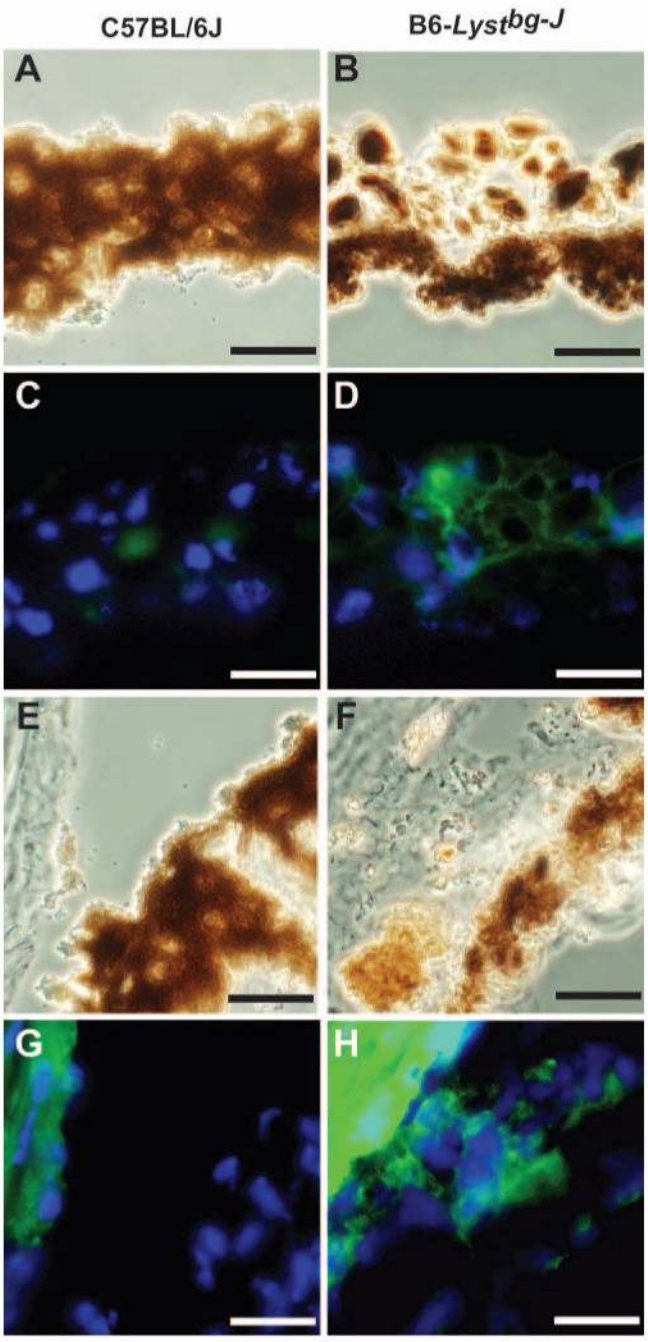

Figure 5.
Accumulations in eyes of B6-*Lyst*$^{bg-J}$ homozygotes contain epitopes characteristic of exfoliative material. Cryosections of wild-type C57BL/6J (*left*) and mutant B6-*Lyst*$^{bg-J}$ (*right*) eyes labeled with anti–fibrillin-1 antibody (*green*) and DAPI (*blue*). (**A**, **B**) Phase-contrast images of iris sections. (**C**, **D**) B6-*Lyst*$^{bg-J}$ eyes are characterized by anti–fibrillin-1–positive material on the surface of the iris. (**E**, **F**) Phase-contrast images of the iridocorneal angle. (**D**, **H**) B6-*Lyst*$^{bg-J}$ eyes are characterized by anti–fibrillin-1–positive material accumulations in the iridocorneal angle. Nonspecific labeling of the cornea is also evident in (**G**, **H**). Scale bars, 25 μm. All eyes were taken from age-matched 6-month-old mice.

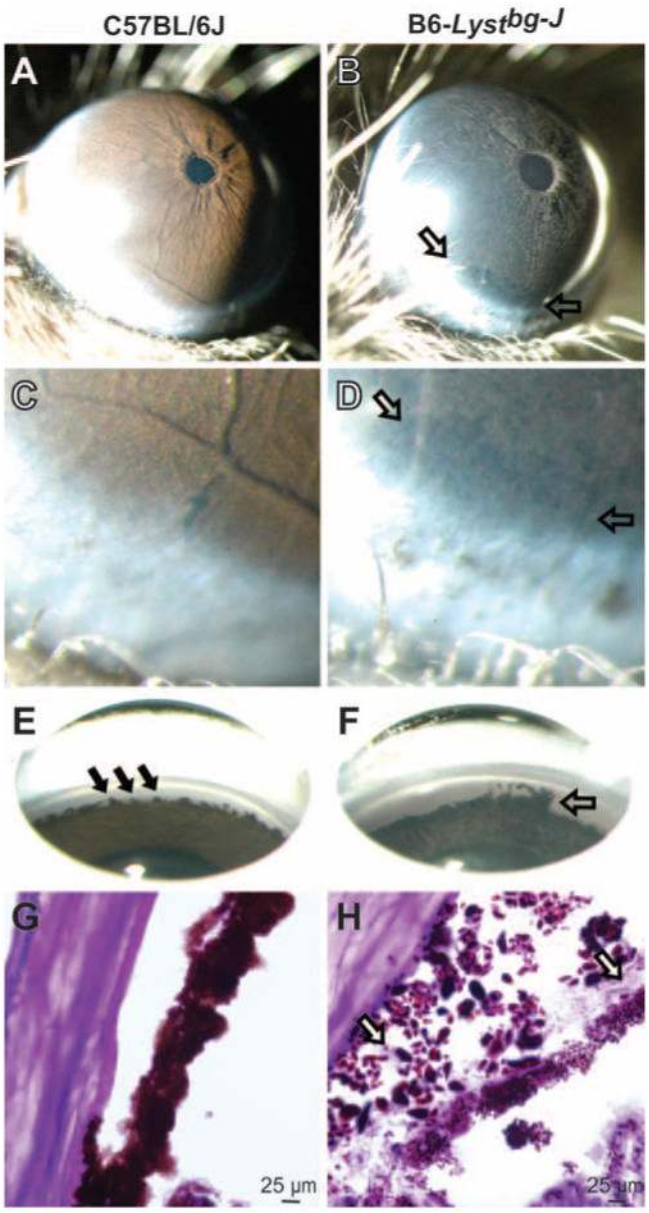

Figure 6.

The iridocorneal angle of the B6-*Lyst*$^{bg-J}$ homozygote is occluded by dispersed pigment and debris. Slit-lamp, gonioscopic, and histologic images of the iridocorneal angle of wild-type C57BL/6J (*left*) and mutant B6-*Lyst*$^{bg-J}$ (*right*) eyes. (**A**) Slit-lamp image with broad beam illumination of the wild-type C57BL/6J eye showing the normal appearance of the inferior anterior chamber. (**B**) Mutant B6-*Lyst*$^{bg-J}$ eyes show pronounced pigment accumulation in the iridocorneal angle that is particularly pronounced inferiorly (*open arrows*). Higher magnification images of the same eyes accentuating angle features of (**C**) C57BL/6J and (**D**) B6-*Lyst*$^{bg-J}$ eyes. The dispersed pigment has a distinctly rounded appearance, likely indicating the presence of pigment-engulfed phagocytic clump cells. (**E**) Gonioscopic appearance of the inferior C57BL/6J iridocorneal angle. Numerous fine iris strands are apparent (*solid arrows*). (**F**) Gonioscopic appearance of the inferior B6-*Lyst*$^{bg-J}$ iridocorneal angle. A large fingerlike clump of dispersed pigment is evident (*open arrow*), and the dispersed pigment obscures views

of finer features such as the iris strands. (**G**) Histologic sections of C57BL/6J eyes stained with PAS show a normal healthy iris and an iridocorneal angle free of pigment and debris. (**H**) Histologic sections of B6-*Lyst*$^{bg\text{-}J}$ eyes stained with PAS show substantial amounts of dispersed pigment and pigment-engulfed macrophages in the iridocorneal angle. PAS-positive material is also evident along the surface of the iris and in the iridocorneal angle (*pink staining, open arrows*). (**A**, **B**) Collected at 25× magnification, cropped, and reduced. (**C–F**) Collected at 40× magnification, with less image reduction.

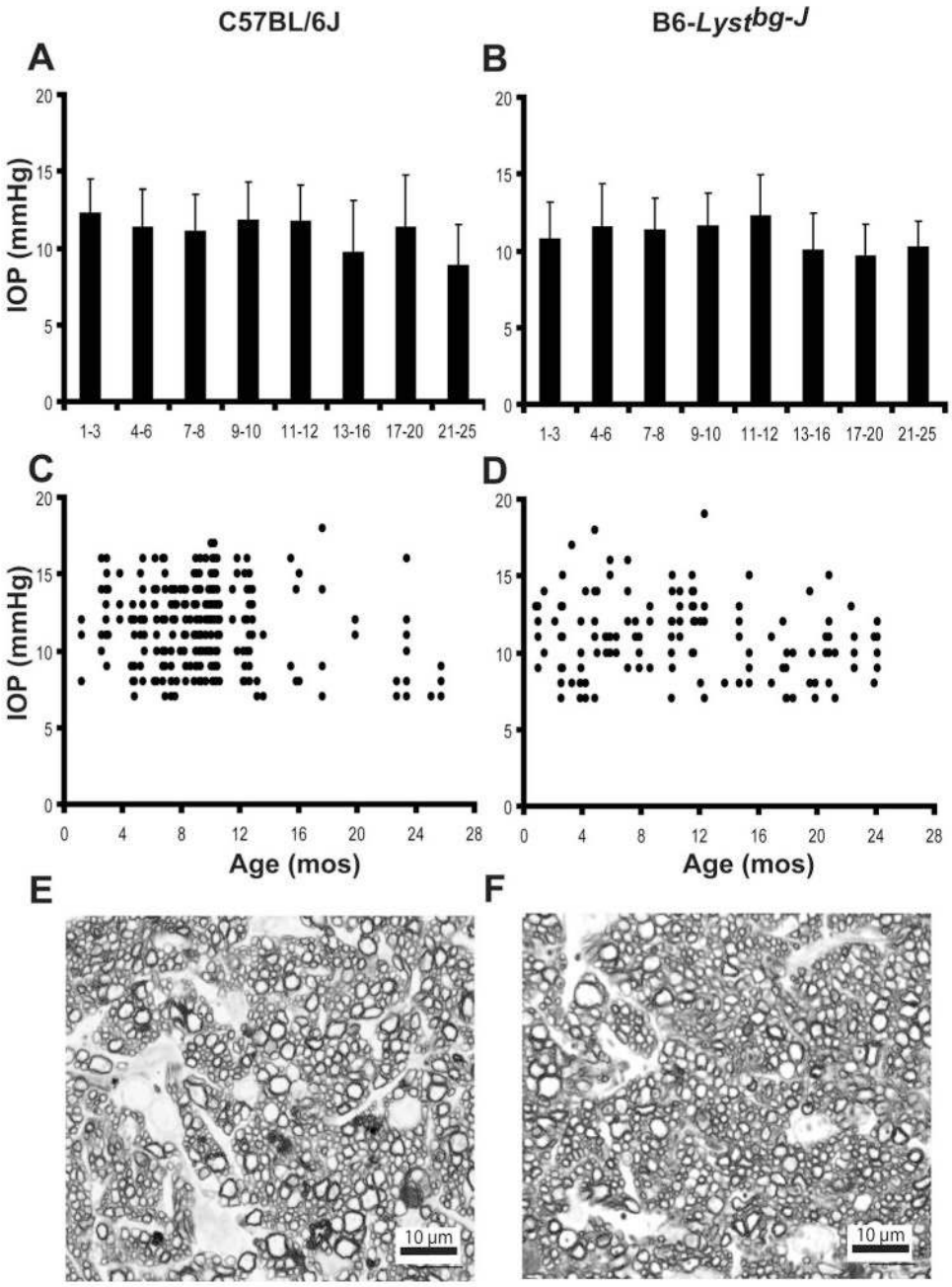

Figure 7.

B6-*Lyst*$^{bg-J}$ homozygotes do not develop indices of glaucoma. IOP and optic nerve phenotypes of wild-type C57BL/6J (*left*) and mutant B6-*Lyst*$^{bg-J}$ (*right*) mice. IOP profiles of aging cohorts, represented as (**A**, **B**) group data (mean ± SD) and (**C**, **D**) individual measurements. (**E**, **F**) Representative optic nerve cross-sections from 12-month-old mice stained with PPD.

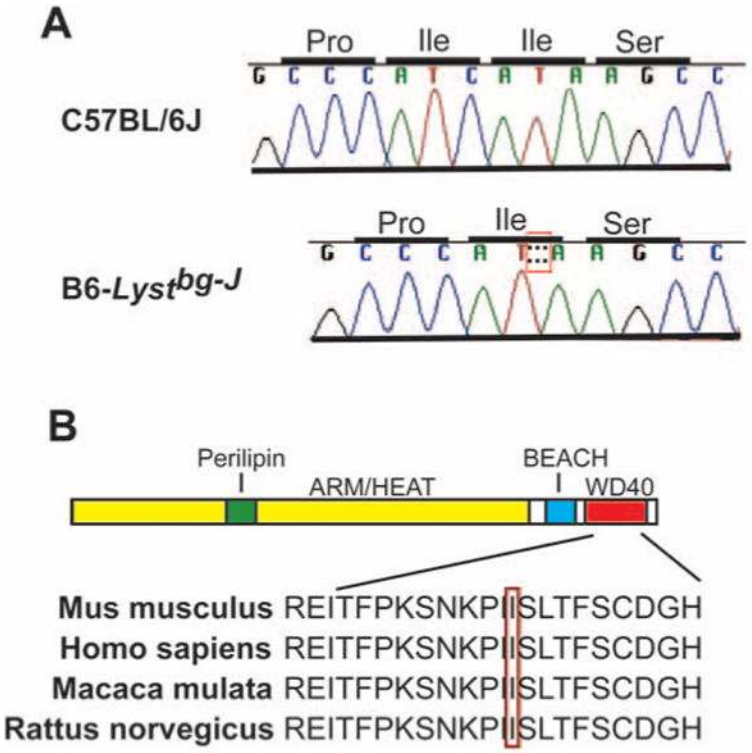

Figure 8.
The *Lyst*$^{bg-J}$ mutation disrupts a conserved protein-protein interaction motif. (**A**) The *bg-J* mutation is a 3-bp deletion in exon 54. (**B**) As a consequence of the *bg-J* mutation, an evolutionarily conserved isoleucine in the seventh repeat of the WD40 domain is predicted to be deleted (*red box*). Recognizable domains of the LYST protein include ARM/HEAT (*yellow*), perilipin (*green*), BEACH (*blue*), and WD40 (*red*).